

Estimation and Prediction of Deterministic Human Intent Signal to augment Haptic Glove aided Control of Robotic Hand

Rajesh Kumar*, Pimmy Gandotra†, Brejesh Lall†, Arzad A. Kherani‡, Sudipto Mukherjee*

Abstract—The paper focuses on Haptic Glove (HG) based control of a Robotic Hand (RH) executing in-hand manipulation. A control algorithm is presented to allow the RH relocate the object held to a goal pose. The motion signals for both the HG and the RH are high dimensional. The RH kinematics is usually different from the HG kinematics. The variability of kinematics of the two devices, added with the incomplete information about the human hand kinematics result in difficulty in direct mapping of the high dimensional motion signal of the HG to the RH. Hence, a method is proposed to estimate the human intent from the high dimensional HG motion signal and reconstruct the signal at the RH to ensure object relocation. It is also shown that the lag in synthesis of the motion signal of the human hand added with the control latency of the RH leads to a requirement of the prediction of the human intent signal. Then, a recurrent neural network (RNN) is proposed to predict the human intent signal ahead of time.

Index Terms—Haptic Glove, Robotic Hand, Tele-operation, Recurrent Neural Network, Estimation Techniques, High-Dimensional Signal Mapping

I. INTRODUCTION

Tele-operation systems have been focus of research for decades. The initial research (since the 1940s) in robotics was inspired by the probable development of robust tele-operation architectures and have continued to develop since then [1], [2]. Tele-operation in robots have been developed in various domains, including remote surgery [3]–[6], remote diagnosis [7]–[9], space robotics [10], [11]; and handling of hazardous materials [12], [13]. The ultimate goal is to control the robot based on the intention of the human. The tele-operation strategies draw on developments in remote sensing [14] and tele-presence [15].

The robot control can be supervisory [16], [17], or semi-autonomous [18]–[23]. During supervisory and semi-autonomous control of the robot, the human commands the motion of the robot while the robot executes the motion. The tele-operation algorithms have been primarily demonstrated using serial robotic arms [24], mobile robots [25], and Unmanned Aerial Vehicles (UAVs) [26]. The desired motion from the human is mapped to the robotic end. Researchers have demonstrated tracking of the end effector motion (of the robotic arm) [27]–[29], and the combination of human motion and the applied force (impedance-based methods [30]–[34]). The robotic human and robotic motion is usually coupled with the necessity to perform a desired task. Execution of this task invariably requires the robot to interact with the environment [35]. The early modes of supervisory control

were limited to control based on audio, visual and force feedback signals of the robotic motion [36], [37]. However, with the advent of haptic based joysticks [38], [39], HGs [40]–[42], different mechanisms of tactile feedback [43]–[46] were also introduced. This allows the humans to get an approximate feel of the robot interacting with the environment. The above-said architectures are usually deployed with serial robotic arms performing the manipulation. In order to manipulate the object or to perform certain tasks, the serial robotic arms are usually appended by grippers that hold and grip the object [9], [47]–[49]. Apart from generation of signals representing the human motion [50] and subsequent control, different Electromyography (EMG) signals [51]–[54], and brain-computer interfacing (BCI) signals [55]–[59] have also been used to control the robot. The research focused on rendering the muscle and the brain signals of the human user by eliminating noise in order to estimate the human intention.

Apart from the development of the haptic interfaces and sensor modules to detect human motion [46], [60]–[62]; there has been a widespread interest in deploying estimation [63]–[65] and prediction [66] algorithms to generate both motion commands and control signals for active robotic control. Predictor based algorithms are useful to mitigate control and transmission delays during the control of the robot. For instance, Munir et al. [67] deployed a Modified Smith Detector algorithm to deploy a tele-operation system. Hauser [68] proposed a Gaussian Mixture Autoregression model (GMA) to predict the user intent signal generated from the 2D motion of a cursor in order to operate a 6 Degrees of Freedom (DoF) robotic arm. Xi et al. [69] proposed a task parameterized Hidden Markov model to encode the signal containing information about the human intent. Model-based predictive methods of the signals containing information about the human (master) intent are popular [70], [71]. Neural Network-based approaches have been utilised to predict the master side (human side) intent [72]–[74]. Neural network-based methods have also been used in reinforcement learning [75], [76] and inverse reinforcement learning methods (including deep imitation learning) [77]–[80]. Methods have also been proposed to predict the force feedback signal from the end of the robot [81]. Methods have also been proposed to ensure stability of the master - slave system amidst delays during tele-operation [82].

Although numerous modules have been deployed for analysis, estimation and prediction of the signals transmitted during tele-operation for pick and place modules with serial robotic arms, in-hand manipulation maneuvers constituting precision

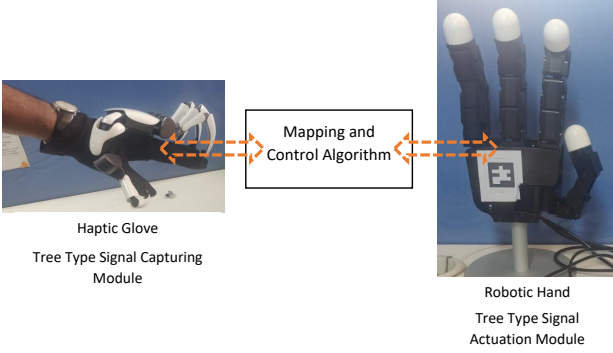


Fig. 1. The mapping and control block needs to be synthesized in the paper.

grasp modes are limited [83]. Precision grasp based in-hand manipulation recruits motion of the fingertips of a RH such that the object moves relative to the palm. Numerous hands focus on standalone in-hand manipulation precision grasp based manipulation behaviour [84], [85]. Although in-hand manipulation has visual similarity to the traditional pick and place operations using serial robots, the former demands precise control of the motion of each of the fingertips and the force applied by the fingertips in order to ensure that the object does not slip from the grip. Difficulty is encountered in mapping the combination of the two measures, force and motion, from the human hand to the RH. This is compounded by the RHs developed having kinematics different from that of the human hand.

For the case of the RHs, multiple fingertips combine to manipulate the object. The motion commands to the joints of the RH lead to a finite motion of the fingertips. Correspondingly, the motion of the fingers of the human hand is captured at intervals via the HG. Although the HG motion signal represents the motion of the joints of the human fingers, the signal usually does not represent the complete object kinematics. As the kinematic architecture of the RH is seldom similar to that of the human hand, there is no one to one mapping between the two signals (the joint motion input to the RH and the joint motion output from the HG). Apart from the kinematic variance of the two devices, the interaction of the two with real world objects is also dissimilar. The two manipulator-object interactions differ in contact stiffness and local friction characteristics, necessitating different interpretations of the two block of signals in discussion. Although, the signal from the HG contains important information of the joint motion, the same cannot be transmitted directly to the RH. Rather, an appropriate encoding - decoding and subsequent control strategy is needed to transform the signal from the human into an interpretable human intent. Then, a subsequent strategy should be deployed to estimate the input signal to the RH in order to complete the desired map. Dex-Pilot [83] presented a strategy to perform in-hand manipulation of the object focusing on estimating a template of motion of the human fingertips and subsequent training for a particular task. It shall also be detailed later in the paper that due to a significant initial acceleration phase in the human motion, the motion of the robot tends to lag the motion of the human user. Hence,

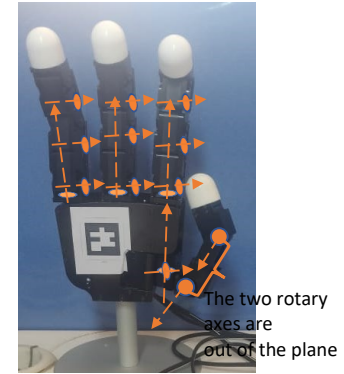


Fig. 2. Allegro RH with 16 actuated joints. The arrows representative of the axes of rotation, orthogonal to the circle.

a learning algorithm is proposed to generate a human intent signal based on the measurements to mitigate the latency.

The proposed system architecture consists of two subsystems, the RH [86] and the other is the HG (Fig. 1). The human user wears HG, which senses the human motion at ' k ' joints such that $k \leq n$, where ' n ' is the number of finger joints on the human hand which exactly characterises the motion of all the fingers. It means that the HG does not exactly characterise the motion of the human fingertips, like in the case of Dexmo Haptic Glove (DHG) [87] that senses the motion signal at 11 points on the human hand as opposed to 19 odd joint actuation in the human finger. Also, the HG restricts motion of the human fingers at k_2 joints, such that $k_2 \leq k$ (using a restrictive torque). The other subsystem is the RH consisting of k_3 active joints with p serial chains out of the tree type robotic system [88]. The RH and the HG have different DH parameters (Denavit-Hartenberg) and might be differently oriented (for instance, during the experiment, the Allegro RH [86] (Fig. 2) is right oriented whereas the DHG is left-oriented). The only similarity between the two robotic systems seems to be that the two are tree type robotic systems with serial chains. We aim however to map the intent of the human using the HG and deploy control signals to the RH to achieve the intended manipulation. The contributions of the work can be stated as:

- Synthesis of a control algorithm such that RH achieves the desired goal pose for the object
- Determining the desired goal pose of the object being manipulated by the RH based on the HG joint motion
- Synthesis of a predictor of the goal pose, based on an intent template to leverage control latency

II. FEEDBACK CONTROL ARCHITECTURE FOR STICKING MANIPULATION OF THE OBJECT

Consider an RH with k_3 actuated joints and p serial chains within the tree (Fig. 3). Each of the serial chain holds needs to interact with the object and perform manipulation such that the goal (target) object pose is reached. The manipulation considered in this paper is a rotation of the object. Additionally, the k_3 actuated joints are torque/ current-controlled (like the Allegro RH). Let \mathbf{r}_i be the vector connecting a suitable point

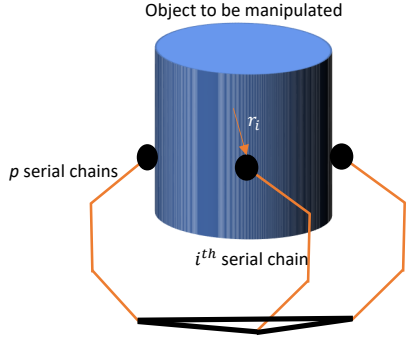


Fig. 3. A tree type robot contacting the object.

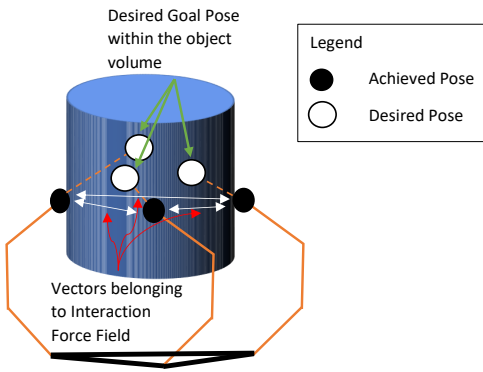


Fig. 4. Due to end effector impedance, the fingertips remain on the object surface with a residual force.

on the object to the i^{th} ($1 \leq i \leq p$) contact point on the surface of the object. It is known that the equations governing forces that can be applied by the fingertips of the RH form an under-specified set of equations, with null space solutions. [89].

$$\underbrace{\begin{bmatrix} \mathbf{1}_{3 \times 3} & \mathbf{1}_{3 \times 3} & \dots & \mathbf{1}_{3 \times 3} \\ \tilde{\mathbf{r}}_1 & \tilde{\mathbf{r}}_2 & \dots & \tilde{\mathbf{r}}_p \end{bmatrix}}_{\mathbf{G}} \underbrace{\begin{bmatrix} \mathbf{f}_1 \\ \mathbf{f}_2 \\ \vdots \\ \mathbf{f}_p \end{bmatrix}}_{\mathbf{F}} = \mathcal{W} \quad (1)$$

where $\tilde{\mathbf{r}}_i$ refers to the cross product matrix corresponding to the vector \mathbf{r}_i , and $\mathbf{1}_{3 \times 3}$ represents the 3×3 identity matrix. The vector \mathbf{f}_i refers to the force applied by the fingertips on the surface of the object by the i^{th} fingertip. The vector $\mathcal{W} \in \mathbb{R}^6$ refers to the net forces and moments applied to the object by the fingertips [90]. The net object dynamics is represented as:

$$\begin{bmatrix} \mathbf{M}_o \mathbf{a}_o \\ \mathbf{I}_o \dot{\omega}_o + \omega_o \times \mathbf{I}_o \omega_o \end{bmatrix} = \mathcal{W} \quad (2)$$

The term \mathbf{M}_o is the mass of the object, \mathbf{a}_o the linear acceleration of the object, \mathbf{I}_o the moment of inertia tensor of the object, and ω_o is the angular velocity of the object. It is known that the solution to the grasp map (Eq. (1)) is a combination of two vector fields. The fingertip forces belonging to the

equilibrating force field imparts motion to the object. However, the interaction force field generates the null solutions. Though motion is not imparted, assigning suitable null forces leads to improvement of the contact condition.

It is also known that the force vectors belonging to the interaction force field can be spanned using the vectors joining the fingertips. Consider the case shown in Fig. 4, which is a three-point grasp. The general solution to the force field [91], [92] is usually represented as:

$$\mathbf{F} = \mathbf{G}^+ \mathcal{W} + \sum_{i=1}^{3p-6} \alpha_i \mathbf{NS}(\mathbf{G}) \quad (3)$$

where $p > 2$, $\mathbf{NS}(\mathbf{G})$ represents the null space of the matrix \mathbf{G} (the grasp matrix as per Eq. (1)), \mathbf{G}^+ represents the Moore-Penrose Pseudo Inverse [93] of the matrix \mathbf{G} , and α_i are assignable scalars to the null space matrix. The dynamics of the RH, as with all kinematic chains, with the vector \mathbf{q} as the joint state of the robot is generally represented as:

$$\mathbf{M} \ddot{\mathbf{q}} + \mathbf{C}(\mathbf{q}, \dot{\mathbf{q}}) + \mathbf{g}(\mathbf{q}) = \tau - \mathbf{J}^T \mathbf{F}_{\text{ext}} \quad (4)$$

where \mathbf{M} refers to the mass matrix of the robot, \mathbf{C} refers to the Coriolis term of the dynamics, $\mathbf{g}(\mathbf{q})$ refers to the gravity compensation term of the robot, τ vector refers to the torque applied at the actuated joints. The vector \mathbf{F}_{ext} is the force applied to the end effectors. Derivation for dynamics of tree type robots in the same form is available as well [88]. Consider the robot grasping the object with individual fingertips controlled under impedance control. The torque vector τ is determined as:

$$\begin{aligned} \tau = & \mathbf{K}(\mathbf{q}_{\text{des}} - \mathbf{q}) + \mathbf{D}(\dot{\mathbf{q}}_{\text{des}} - \dot{\mathbf{q}}) + \mathbf{M} \ddot{\mathbf{q}}_{\text{des}} + \mathbf{C}(\mathbf{q}_{\text{des}}, \dot{\mathbf{q}}_{\text{des}}) \\ & + \mathbf{g}(\mathbf{q}_{\text{des}}) \end{aligned} \quad (5)$$

where \mathbf{q}_{des} is the desired motion of the joints required to achieve the desired position. The matrices \mathbf{K} , \mathbf{D} are the gain matrices for robotic control [94]. Another well known result is that when motors with high gear ratio are deployed, the system dynamics (coefficients for time derivatives of the joint states) can be neglected as disturbance. The impedance control hence allows an unconstrained end effector (fingertip) to achieve the set goal pose. However, when the robotic fingertip interacts with the object, the force applied by the fingertip on the object is proportional to the difference in the achieved pose and the desired pose.

As stated earlier, the interaction force components can be assigned without affecting the motion of the object. The goal pose of the fingertips are set to be within the object in order to enhance the contact condition. This is shown schematically in Fig. 4, where the goal pose of the fingertips is within the object volume. However, due to the constraint of the object in between, the fingertips cannot achieve the desired pose. The interaction force field can be viably transmitted using the projection along the line joining the fingertips on the surface of the object.

Once viable contact conditions are achieved, a kinematic resolved rate motion controller is used. It is also known that any rigid body rotation is represented as an element of the

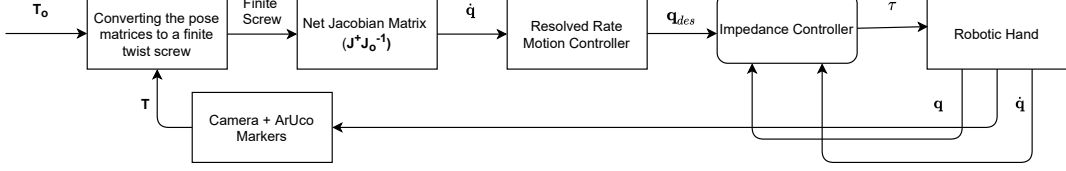


Fig. 5. Representation of the control algorithm to achieve the desired object pose using the RH

$\mathbb{SO}(3)$ manifold [95], and any general rigid body motion is represented as an element of the $\mathbb{SE}(3)$ manifold [96]. The goal pose and the current pose of the object be defined as an element of the $\mathbb{SE}(3)$ manifold. A general pose matrix T is represented as: $T \equiv \begin{bmatrix} R & o \\ 0 & 1 \end{bmatrix} \mid R \in \mathbb{R}^{3 \times 3}, o \in \mathbb{R}^3, R^T R = \mathbf{1}_{3 \times 3}, \det(R) = 1\}$. The twist screw $\$_o \in \mathbb{R}^6$ represents the twist representation (combination of the linear and the angular velocity) relating the current object pose (T) to the desired object pose (T_o). The details for the determination of the screw $\$_o$ to translate between two object pose matrices can be referred to in the literature [97]. It is known that the least energy geodesic is determined by the screw rotation between the initial and the desired poses [97]. The object level screw rotation trajectory is utilised to transit the object from the initial pose to the desired goal pose. The end effector twist of the i^{th} finger of the RH is quantified as:

$$\$_i = J_i \dot{q}_i \quad (6)$$

where the matrix J_i is the Jacobian matrix relating the joint rates to the twist of the end effector twist of the i^{th} fingertip ($\$_i$). The vector q_i refers to the joint angles of the active joints of the i^{th} tree, whereas as the vector $q = [q_1^T, \dots, q_p^T]^T$. So, the vector containing the twists of all the fingertips for the robot reduce to:

$$\underbrace{\begin{bmatrix} \$_1 \\ \$_2 \\ \vdots \\ \$_p \end{bmatrix}}_{\$_{RH}} = \underbrace{\begin{bmatrix} J_1 & 0 & \dots & 0 \\ 0 & J_2 & \dots & 0 \\ \dots & \dots & \dots & \dots \\ 0 & 0 & \dots & J_p \end{bmatrix}}_J \dot{q} \quad (7)$$

Given the desired twist of the object $\$_o$, the twist of the i^{th} fingertip of the RH is quantified as:

$$\$_i = \underbrace{\begin{bmatrix} \mathbf{1}_{3 \times 3} & \mathbf{0}_{3 \times 3} \\ -\tilde{r}_i & \mathbf{1}_{3 \times 3} \end{bmatrix}}_{J_{oi}} \$_o \quad (8)$$

The Eq. (8) can then be extended to p serial chains as:

$$\underbrace{\begin{bmatrix} \$_1 \\ \$_2 \\ \vdots \\ \$_p \end{bmatrix}}_{\$_{RH}} = \underbrace{\begin{bmatrix} J_{o1} \\ J_{o2} \\ \vdots \\ J_{op} \end{bmatrix}}_{J_o} \$_o \quad (9)$$

The Eq. (7) and the Eq. (9) can be collated as:

$$\dot{q} = J^+ J_o^{-1} \$_o \quad (10)$$

Utilising the standard resolved rate motion approximation, the subsequent incremental goal pose is determined using the control equation:

$$\dot{q}_{des} = q + \eta \dot{q} \Delta t \quad (11)$$

Following which, the desired joint angle vector presented in Eq. (11) is utilised in Eq. (5) to compute the actuation torques. The net control algorithm is depicted pictorially in Fig. 5. The object twist is derived from the desired object pose matrix and the current object pose matrix (determined from an external camera system using vision techniques like ArUCo Markers [98]). Having established a control algorithm to ensure that the robotic fingertips result in the RH achieving the desired object pose, we focus on the synthesis of the goal object pose from the signals from the human wearing the HG.

III. SYNTHESIS OF THE HUMAN INTENT BY SUPERPOSITION OF SERIAL CHAIN KINEMATICS

As noted earlier, the only kinematic similarity between the RH and the HG is both are tree-type robotic system with serial chains. Further, the joint encoders on the HG do not exactly characterise the exact motion of the human fingertips. A heuristic is proposed here for superposition of the kinematics of the serial chains of the HG to the kinematics of the serial chains of the RH. The data flow in relating the input signal on the HG to the motion of the object on the RH is presented schematically in Fig. 6. Consider the mapping of the fingertip of the i^{th} serial chain of RH and the i^{th} serial chain of the HG. The first-order differential kinematics of the i^{th} fingertip of the RH is represented as:

$$\$_i = \sum_{j=1}^{k_3} \$_{ij} \dot{\theta}_j \quad (12)$$

where $\$_{ij}$ represents the screw rotation of the j^{th} joint of the i^{th} chain. The kinematics of the i^{th} serial chain, including the active joints of the HG on the i^{th} serial chain yields the hypothetical first order kinematics of the hand as:

$$\$'_i = \sum_{j=1}^k \$'_{ij} \dot{\theta}'_j \quad (13)$$

The vector $\$'_{ij}$ represents the equivalent screw motion of the active joint on the HG to the RH. For all the k hypothetical kinematics of the HG on the RH, the estimated object screw motion is characterised as the minimum norm rigid body motion, quantified as:

$$\$'_o = J_o^+ \$_{HG} \quad (14)$$

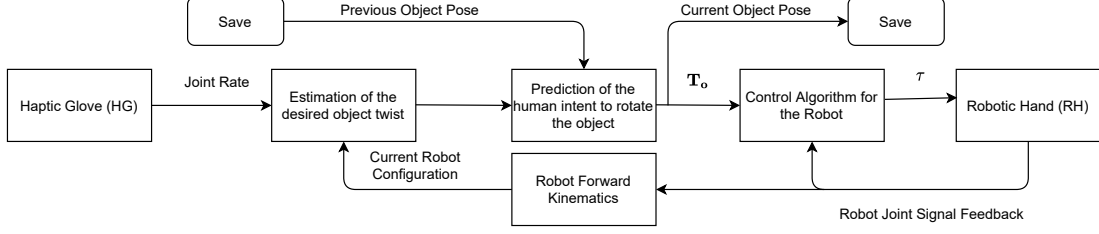


Fig. 6. Representation of the algorithm to achieve the desired object pose using the input from HG

The vector $\$_{HG}$ is quantified as:

$$\$_{HG} = \begin{bmatrix} \$'_1 \\ \vdots \\ \$'_p \end{bmatrix} \quad (15)$$

The instantaneous linear velocity and the angular velocity of a point on the object can be derived based on the screw representation as $[\mathbf{v}, \omega] = \$'_o$. Upto a time t , knowing the hypothetical twist motion, the motion of the object can be synthesised as: $d = \int_0^t \mathbf{v} dt$, and $\Delta\theta = \int_0^t \omega dt$. Subsequently, the goal transformation matrix is repeatedly synthesised as: $\mathbf{T}_o = \begin{bmatrix} \mathbf{R} & \mathbf{d} \\ \mathbf{0} & 1 \end{bmatrix}$, with the matrix $\mathbf{R} = \mathbf{1}_{3 \times 3} + \mathbf{E} \sin \theta + \mathbf{E}^2 (1 - \cos \theta)$. The matrix \mathbf{E} is defined as: $\mathbf{E} = \begin{bmatrix} 0 & -\Delta\theta_z & \Delta\theta_y \\ \Delta\theta_z & 0 & -\Delta\theta_x \\ -\Delta\theta_y & \Delta\theta_x & 0 \end{bmatrix}$, where $\Delta\theta = \begin{bmatrix} \Delta\theta_x \\ \Delta\theta_y \\ \Delta\theta_z \end{bmatrix}$, $\theta = \|\Delta\theta\|_2$. In this formulation, the integral effect of the hypothetical twist screw is used to repeatedly determine the human intention to manipulate the object. Often the intent of prehensile manipulation is primarily a rotation, in which case the velocity terms \mathbf{v} are equated to 0.

It shall be seen that the human intent coded as per this methodology accumulates the effect of the instantaneous motion of the human finger joints. We introduce the observed knowledge that the human tendency is to follow a ‘sigmoid’ like curve while manipulating objects. This includes an acceleration phase associated with only a small cumulative rotation (or displacement of the hypothetical/real object), followed by a large displacement period and then a small motion and large deceleration period. At the same time, the RH joints require a finite time to accelerate to follow the goal trajectory. The cumulative effect of the human intent, the goal pose, is evident only after the deceleration phase is initiated. This leads to a lag in the motion of the RH vis-à-vis, the signal captured by HG. The time delay between the feedback at the HG and visual feedback of the RH is counter intuitive to a teleoperator and is usually overcome by significant on the job training.

IV. PREDICTION OF THE GOAL POSE

To minimise the effect of control latency, a method which generates a prediction in finite but small time is needed. We propose to use the heuristic that the humans deploy prehensile manipulation in repeated tasks. Thereby, a Recurrent Neural Network (RNN), which have traditionally been used for the

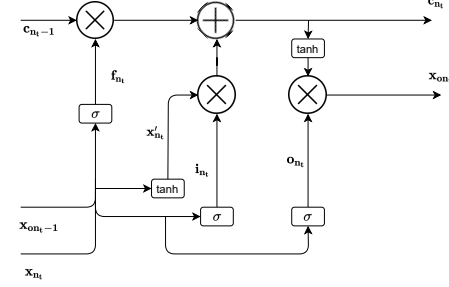


Fig. 7. Representation of an LSTM network node

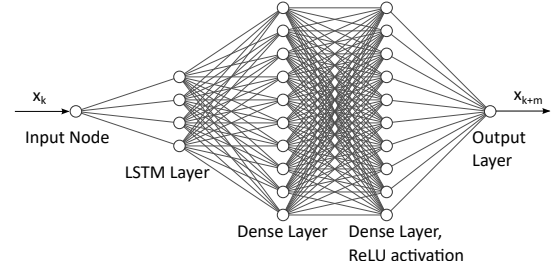


Fig. 8. Representation of the used neural network

processing of sequential data for a wide variety of signals [99]–[103] based prediction methodology is proposed.

The encoded motion of the joints of the human fingers has been reformulated as a sequence of integral solutions in the previous section. The integral solution at any time instance ‘ t ’ is based on the current estimate and accumulation of the prior trajectory, giving rise to the necessity of sequence learning. Hence, sequence based RNN models are used to predict a futuristic estimate. The memory cell feature of the Long Short Term Memory (LSTM) based networks are useful for this case, as the human intended motion of the object follow three characteristic features within the signal. The LSTM network also retains characteristic components of the signal while massaging the issue of vanishing gradient in traditional RNNs [104]. As shown in the example later, the signal includes a slow start, a fast growth and then a saturation. This feature is repeated in the signal. The network is hence used to train the three features and output is the goal pose, a finite time in the future.

For a rotational motion of the object with respect to a coordinate frame, the vector $\Delta\theta$ represents the net motion of the object. Let us assume that the term $\Delta\theta_x$ at an instance t is labelled as $\Delta\theta_{x_{n_t}}$. Also, consider a sequence consisting of ‘ r ’

elements: $\mathbf{x}_{n_t} = \{\Delta\theta_{x_{n_t-r}}, \Delta\theta_{x_{n_t-r+1}}, \dots, \Delta\theta_{x_{n_t}}\}$, where n_t corresponds to the element index at time instance t . So, the sequence \mathbf{x}_{n_t} consists of r elements sampled sequentially from the signal upto time t . Similarly, for the other two elements, the sequences \mathbf{y}_{n_t} and \mathbf{z}_{n_t} can be synthesized.

Corresponding to the vector \mathbf{x}_{n_t} , a scalar $x_{n_t+m_t}$ is to be synthesized such that it is the predicted $(n_t + m_t)^{th}$ element of the sequence, where ' m_t ' is suitably selected based on the time of prediction. A Long Short Term Memory (LSTM) [105] based neural network is synthesized such that the network predicts a state given the prior sequence of data. The input to the LSTM network is \mathbf{x}_{n_t} . An LSTM network consists of different gates to train a network on the sequence, comprising of the forget gate, input gate, and the output gate is presented in Fig. 7. For each iteration of the network (corresponding to the time index t), a sequence containing r elements is used as an input and the prediction estimate corresponding to the $(n_t + m_t)^{th}$ element of the signal is the output. The LSTM network utilises the following equations to predict the output, given an input sequence:

$$\mathbf{x}'_{n_t} = \tanh(\mathbf{W}_1^T [\mathbf{x}_{n_t}^T, \mathbf{x}_{n_t-1}^T]^T) \quad (16)$$

$$\mathbf{i}_{n_t} = \sigma(\mathbf{W}_2^T [\mathbf{x}_{n_t}^T, \mathbf{x}_{n_t-1}^T]^T) \quad (17)$$

$$\mathbf{f}_{n_t} = \sigma(\mathbf{W}_3^T [\mathbf{x}_{n_t}^T, \mathbf{x}_{n_t-1}^T]^T) \quad (18)$$

$$\mathbf{c}_{n_t} = \mathbf{i}_{n_t} \circledast \mathbf{x}'_{n_t} + \mathbf{f}_{n_t} \circledast \mathbf{c}_{n_t-1} \quad (19)$$

$$\mathbf{o}_{n_t} = \sigma(\mathbf{W}_4^T [\mathbf{x}_{n_t}^T, \mathbf{x}_{n_t-1}^T]^T) \quad (20)$$

$$\mathbf{x}_{n_t} = \mathbf{i}_{n_t} \circledast \mathbf{x}'_{n_t} + \mathbf{f}_{n_t} \circledast \mathbf{c}_{n_t-1} \quad (21)$$

where \circledast represents element wise multiplication. The matrices \mathbf{W}_i constitute the training parameters and the symbol σ represents the sigmoid function [104]. The vector \mathbf{f}_{n_t} represents the output vector from the forget gate, the vector \mathbf{i}_{n_t} represents the output vector from the input gate, whereas the vector \mathbf{o}_{n_t} represents the output vector from the output gate. The vector \mathbf{c}_{n_t} represents the cell state at time t , indexed as n_t . Subsequently, the vector \mathbf{x}_{n_t} is the output vector from the LSTM block and input to the other subsequent layers. As shown in Fig. 8, two dense layers with 10 nodes are used, one with a 'ReLU' activation [104]. Then a single node output is used to estimate the intent in the sequence after ' m_t ' elements. The backpropagation algorithm is used to successively determine the parameters, to minimize the mean squared error loss function [104].

In the example presented later, a vector consisting of 20 elements (sampled over approximately 1.2 seconds) is used as an input to the network in order to estimate a value after 10 elements (0.6 seconds). A system of overlapping windows is used such that the input signal is sequentially sampled for the past 20 elements. This ensures an overlap of 19 elements for subsequent training samples. Although, the overlapping results in redundancy of the input samples, it allows quick capture during the rapid growth of the signal, which is the one of the three main features of the task. As a general principle of prediction, the number of samples to the input vis-à-vis the futuristic estimate should be selected based on the signal variation.



Fig. 9. Allegro Hand grasping a cubical object

TABLE I
MECHANICAL MOTION RANGE (MMR) FOR THE FOUR JOINTS OF THE THUMB AND THE FOUR FINGERS OF THE ARH IN DEGS

Joint No	Thumb MMR (deg)	Fingers MMR (deg)
1	64.9	66.84
2	84.11	116.52
3	116.52	119.40
4	119.302	116.863

V. EXPERIMENTAL ANALYSIS USING ALLEGRO RH AND THE DHG

The Allegro RH (ARH) consists of four kinematic chains (three fingers and a thumb). Each of the kinematic chain has 4 active joints powered by motors with gear ratio of 1:369. At this ratio, the end effector dynamics can be neglected. The impedance controller produces a desired torque at 333 Hz, whereas the resolved rate motion controller updates the desired joint angle value at 20 Hz. Two fingers and a thumb are used for manipulation. The native resolution of Joint Encoders resolution maps to joint angle of 0.002 degs. However, the signal is transmitted as a 16 bit signal, reducing the resolution to 0.005 degs. The encoders used have a mechanical range of 333.33 degs but individual joints have varying motion ranges arising from hardware intersections as listed in Table I. The torque limits for different joints of the ARH is listed in Table II. Although the desired torque is approached by the control algorithm, the torque capacity of the motor limits the motion performance of joints and hence the robot.

For this paper, the end effector stiffness is constant throughout the manipulation though it could vary with the task. As an embodiment of the control algorithm enumerated in Section II, consider the robot holding a cubical object (as shown in Fig. 9). The true motion of the object is tracked using the ArUco markers pasted on the object. A motion sequence is shown in Fig. 10 using three video snips of change in the object pose. The change of object pose measured about one

TABLE II
LIMITING TORQUE (LT) FOR THE FOUR JOINTS OF THE THUMB AND THE FOUR FINGERS OF THE ARH

Joint No	Thumb LT (Nm)	Fingers LT (Nm)
1	± 0.437	± 0.312
2	± 0.337	± 0.562
3	± 0.225	± 0.375
4	± 0.225	± 0.238

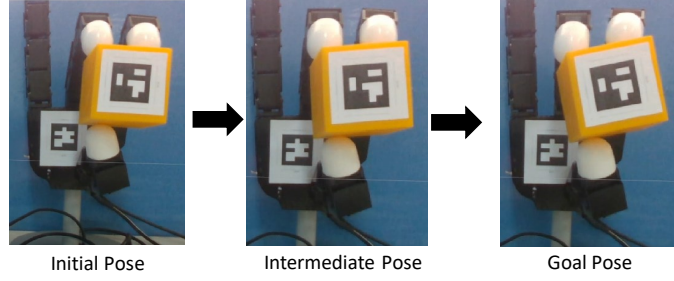


Fig. 10. Motion of the object by the ARH

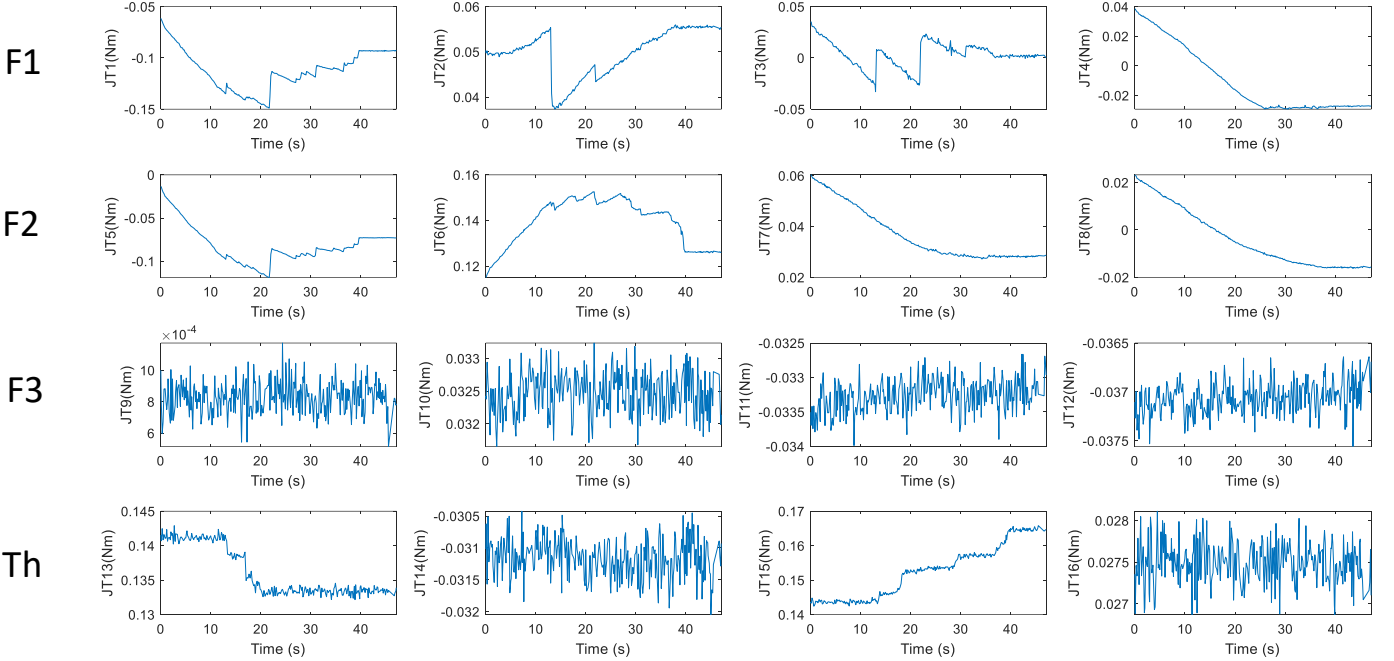


Fig. 11. Variation of the Joint Torque (JT) signal of the 16 actuated joints of the ARH corresponding to the motion in Fig. 10. 'F1' refers to the torque signals of the four joints of the first robotic finger (from right) actuating the object, 'F2' refers to the second finger. 'F3' (third finger) does not hit/ actuate the object, hence the torque signal remains constant. 'Th' refers to the four joints corresponding to the thumb signal

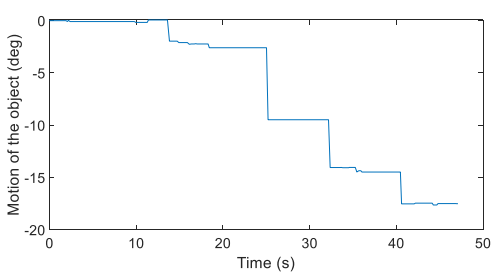


Fig. 12. Motion of the object by the ARH corresponding to Fig. 10

axis is shown in the Fig. 12. The response shows repeated step inputs leading to the desired change in the object pose. The corresponding torque applied by the 16 joints is presented in Fig. 11. The torque applied by the joints for robotic finger 3 (leftmost finger) is constant (with visible signal noise) as the finger does not participate in manipulating the object and

remains free. The variation of the required torque for the rest of the 12 signals can be observed.

Also, consider the DHG which is a tree type chain of five serial chains (four fingers) and a thumb. Each of the fingers has two encoding points, whereas the thumb has three encoding points. The fingers have one encoder recording the bending action while the other encoders record the splitting motion. The DHG encodes the data at the rate of 200 Hz, with a spatial resolution of 0.08 deg for different joints. The signals corresponding to the five joints with bending motion is within the mechanical range of 147 deg, whereas the splitting motion is within 30 deg. The stiffness signal varies from (0 – 0.33 kg-cm/deg). The machine level resolution of the motor torque is 0.005 Nm. The peak torque value is limited to 0.5 Nm. In order to analyse the joint signals from the DHG, a Principal Component Analysis (PCA) [106] was performed by manipulating the object for four test cases. The variation of the joint values for a test motion of the DHG manipulating an object is shown in Fig 13. The corresponding magnitudes of the PCA components for different axes of the 11-D data

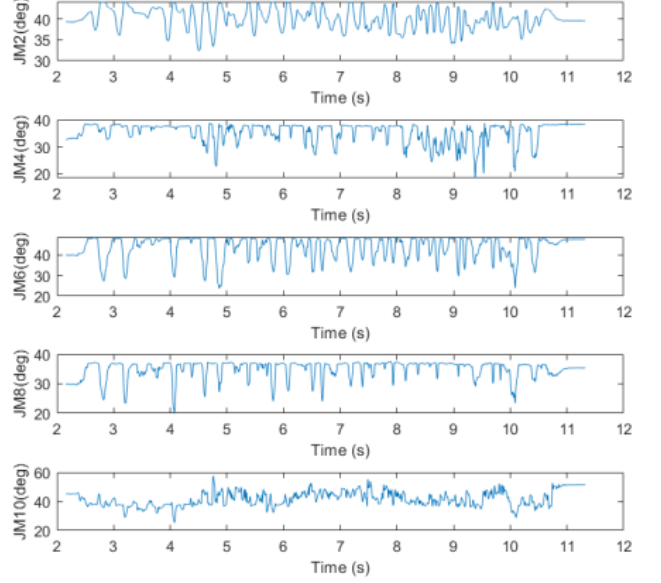
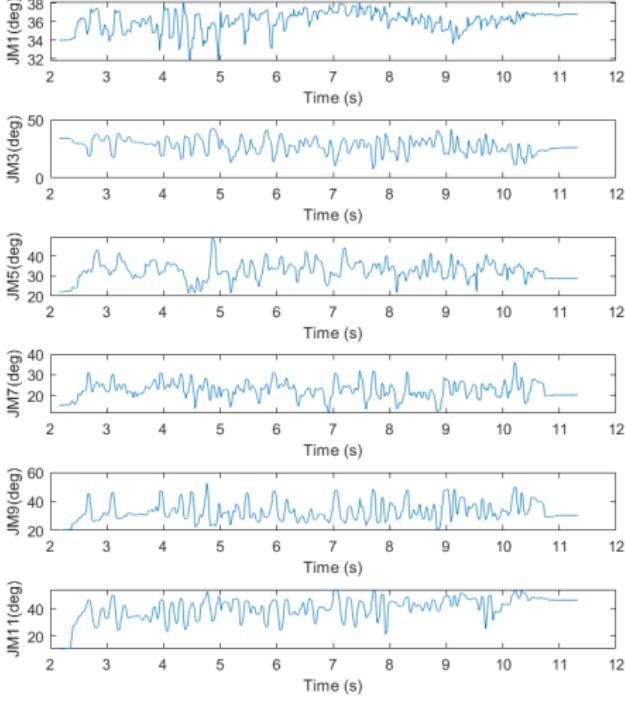


Fig. 13. Variation of the Joint Motion (JM) signal of the 11 joints of the DHG for arbitrary motion with a spherical ball; the joint motion signal for the i^{th} encoder is represented as 'JM i '

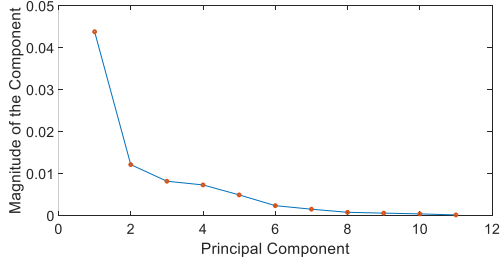


Fig. 14. PCA analysis of the data corresponding to Fig. 13

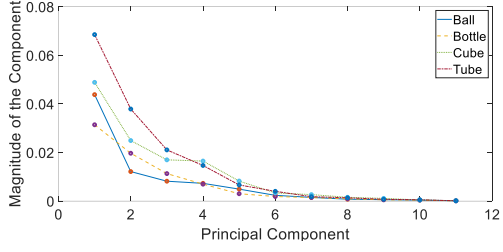


Fig. 15. PCA analysis of the data corresponding for exemplar manipulation of different objects

is presented in Fig 14. For four different test cases, the PCA magnitudes are presented in Fig. 15. It can be seen that for all the cases, the first three components are dominant, with the next three principal values being of lesser significance. This can be attributed to the fact that the primary motion targetted of the object during in-hand manipulation was a general

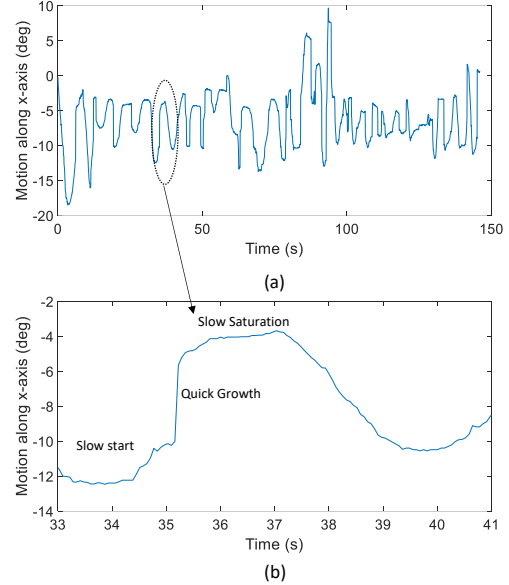


Fig. 16. (a) Exemplar human motion intent of the object (b) Detailed analyses of a single wavelet

rotational motion with parasitic translation motion. Beyond six dimensions, the magnitude of the principal components is negligible, which is consistent with the motion being of a rigid body.

A static stiffness value is used to restrict the DHG at a grasp pose so that the fingers can be restricted. Then the motion of the human fingers is estimated and mapped to a

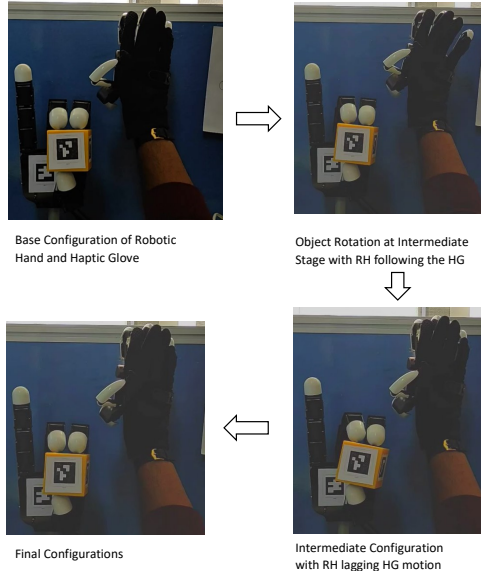


Fig. 17. Intermediate motion of the HG and RH mapping

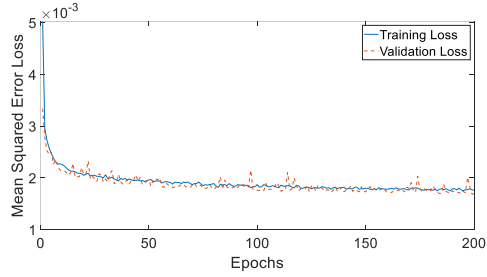


Fig. 18. Mean Squared Error corresponding to the train and the validation data set (rad)

hypothetical motion of the object. The ARH is then controlled to replicate the object motion. The motion of the robotic fingertips followed by capturing the rotational intent in one of the three cartesian directions is presented in Fig. 16. It can be seen that the motion intent of the human to manipulate the object follows an ‘sigmoid’ shaped curve, consisting of a slow growth followed by a quick surge and then a slow saturation. The human intent is small at the initial stages, thereby leading to lag in the motion of the robot (combined with the slow

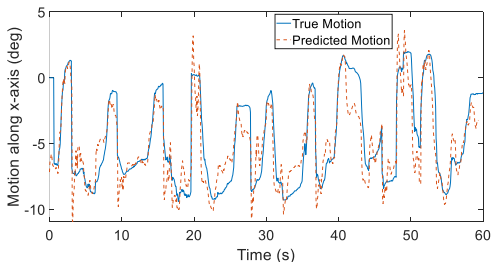


Fig. 19. Comparison of the true data and the predicted data from the algorithm

initial response of the robot). The motion of the RH and the object can be seen in Fig. 17.

It can be seen that the motion of the object by the RH lags the motion of the HG. The RNN network trained on the DHG is then introduced, to predict the goal pose recursively. The corresponding variation of mean squared error loss during training and validation is presented in Fig. 18. Both the losses converge to 0.14 deg. The training data was used to project the motion intent 0.6 seconds into the future. For an example manipulation, the comparison of the predicted variation of the estimate and the true data is presented in Fig. 19. It can be seen that the neural network predicts the desired estimate 0.6 seconds earlier, thereby reducing the control and estimation latency.

VI. CONCLUSION

An introductory development towards HG based control of a kinematically different RH is shown. A stable control algorithm for the RH to relocate the object to a goal pose is presented. Then, a methodology is proposed to deterministically synthesize finger actuation to achieve the desired motion of the object even though the measurement of the hand motion is of a lower dimension. The issue of latency during intent identification and to actuate the robot is enumerated and then managed using a Long Short Term Memory Recurrent Neural Network to predict in the future by leveraging knowledge of time trajectory of typical human actions.

REFERENCES

- [1] P. F. Hokayem and M. W. Spong, “Bilateral teleoperation: An historical survey,” *Automatica*, vol. 42, no. 12, pp. 2035–2057, 2006.
- [2] M. Shahbazi, S. F. Atashzar, and R. V. Patel, “A systematic review of multilateral teleoperation systems,” *IEEE transactions on haptics*, vol. 11, no. 3, pp. 338–356, 2018.
- [3] P. Berthet-Rayne, K. Leibrandt, G. Gras, P. Fraisse, A. Crosnier, and G.-Z. Yang, “Inverse kinematics control methods for redundant snakelike robot teleoperation during minimally invasive surgery,” *IEEE Robotics and Automation Letters*, vol. 3, no. 3, pp. 2501–2508, 2018.
- [4] Z. Wang, I. Reed, and A. M. Fey, “Toward intuitive teleoperation in surgery: Human-centric evaluation of teleoperation algorithms for robotic needle steering,” in *2018 IEEE International Conference on Robotics and Automation (ICRA)*. IEEE, 2018, pp. 5799–5806.
- [5] G. Ateş, R. Majani, and M. I. C. Dede, “Design of a teleoperation scheme with a wearable master for minimally invasive surgery,” in *New Trends in Medical and Service Robotics*. Springer, 2019, pp. 45–53.
- [6] L. Cheng and M. Tavakoli, “Neural network-based physiological organ motion prediction and robot impedance control for teleoperated beating-heart surgery,” *Biomedical Signal Processing and Control*, vol. 66, p. 102423, 2021.
- [7] P. A. Patlan-Rosales and A. Krupa, “Robotic assistance for ultrasound elastography providing autonomous palpation with teleoperation and haptic feedback capabilities,” in *2020 8th IEEE RAS/EMBS International Conference for Biomedical Robotics and Biomechatronics (BioRob)*. IEEE, 2020, pp. 1018–1023.
- [8] M. Al-Badri, S. Ipsen, S. Böttger, and F. Ernst, “Robotic 4d ultrasound solution for real-time visualization and teleoperation,” *Current Directions in Biomedical Engineering*, vol. 3, no. 2, pp. 559–561, 2017.
- [9] G. Yang, H. Lv, Z. Zhang, L. Yang, J. Deng, S. You, J. Du, and H. Yang, “Keep healthcare workers safe: application of teleoperated robot in isolation ward for covid-19 prevention and control,” *Chinese Journal of Mechanical Engineering*, vol. 33, no. 1, pp. 1–4, 2020.
- [10] Z. Liu, Z. Lu, Y. Yang, and P. Huang, “Teleoperation for space manipulator based on complex virtual fixtures,” *Robotics and Autonomous Systems*, vol. 121, p. 103268, 2019.

[11] Z. Wang, H.-K. Lam, B. Xiao, Z. Chen, B. Liang, and T. Zhang, "Event-triggered prescribed-time fuzzy control for space teleoperation systems subject to multiple constraints and uncertainties," *IEEE Transactions on Fuzzy Systems*, 2020.

[12] J. Aleotti, G. Micconi, S. Caselli, G. Benassi, N. Zambelli, M. Bettelli, D. Calestani, and A. Zappettini, "Haptic teleoperation of uav equipped with gamma-ray spectrometer for detection and identification of radioactive materials in industrial plants," in *Factories of the Future*. Springer, Cham, 2019, pp. 197–214.

[13] J. Aleotti, G. Micconi, S. Caselli, G. Benassi, N. Zambelli, M. Bettelli, and A. Zappettini, "Detection of nuclear sources by uav teleoperation using a visuo-haptic augmented reality interface," *Sensors*, vol. 17, no. 10, p. 2234, 2017.

[14] C. R. Jung and J. Scharcanski, "Sharpening dermatological color images in the wavelet domain," *IEEE Journal of Selected Topics in Signal Processing*, vol. 3, no. 1, p. 4, 2009.

[15] D. J. Roberts, A. J. Fairchild, S. P. Campion, J. O'Hare, C. M. Moore, R. Aspin, T. Duckworth, P. Gasparello, and F. Tecchia, "withyou—an experimental end-to-end telepresence system using video-based reconstruction," *IEEE Journal of Selected Topics in Signal Processing*, vol. 9, no. 3, pp. 562–574, 2015.

[16] I. Havoutis and S. Calinon, "Supervisory teleoperation with online learning and optimal control," in *2017 IEEE International Conference on Robotics and Automation (ICRA)*. IEEE, 2017, pp. 1534–1540.

[17] H. Latifee, A. Pervez, J.-H. Ryu, and D. Lee, "Mini-batched online incremental learning through supervisory teleoperation with kinesthetic coupling," in *2020 IEEE International Conference on Robotics and Automation (ICRA)*. IEEE, 2020, pp. 5453–5459.

[18] M. Rubagotti, T. Taunayazov, B. Omarali, and A. Shintemirov, "Semi-autonomous robot teleoperation with obstacle avoidance via model predictive control," *IEEE Robotics and Automation Letters*, vol. 4, no. 3, pp. 2746–2753, 2019.

[19] I. Havoutis and S. Calinon, "Learning from demonstration for semi-autonomous teleoperation," *Autonomous Robots*, vol. 43, no. 3, pp. 713–726, 2019.

[20] D.-H. Zhai and Y. Xia, "Adaptive control of semi-autonomous teleoperation system with asymmetric time-varying delays and input uncertainties," *IEEE transactions on cybernetics*, vol. 47, no. 11, pp. 3621–3633, 2016.

[21] C. Ha, S. Park, J. Her, I. Jang, Y. Lee, G. R. Cho, H. I. Son, and D. Lee, "Whole-body multi-modal semi-autonomous teleoperation of mobile manipulator systems," in *2015 IEEE International Conference on Robotics and Automation (ICRA)*. IEEE, 2015, pp. 164–170.

[22] K. Y. Lui, H. Cho, C. Ha, and D. Lee, "First-person view semi-autonomous teleoperation of cooperative wheeled mobile robots with visuo-haptic feedback," *The International Journal of Robotics Research*, vol. 36, no. 5–7, pp. 840–860, 2017.

[23] W. Li, Z. Li, Y. Liu, L. Ding, J. Wang, H. Gao, and Z. Deng, "Semi-autonomous bilateral teleoperation of six-wheeled mobile robot on soft terrains," *Mechanical Systems and Signal Processing*, vol. 133, p. 106234, 2019.

[24] J. Singh, A. R. Srinivasan, G. Neumann, and A. Kucukyilmaz, "Haptic-guided teleoperation of a 7-dof collaborative robot arm with an identical twin master," *IEEE transactions on haptics*, vol. 13, no. 1, pp. 246–252, 2020.

[25] S. Musić, G. Salvietti, F. Chinello, D. Prattichizzo, S. Hirche *et al.*, "Human–robot team interaction through wearable haptics for cooperative manipulation," *IEEE transactions on haptics*, vol. 12, no. 3, pp. 350–362, 2019.

[26] D. Zhang, G. Yang, and R. P. Khurshid, "Haptic teleoperation of uavs through control barrier functions," *IEEE transactions on haptics*, vol. 13, no. 1, pp. 109–115, 2020.

[27] G. Du, P. Zhang, J. Mai, and Z. Li, "Markerless kinect-based hand tracking for robot teleoperation," *International Journal of Advanced Robotic Systems*, vol. 9, no. 2, p. 36, 2012.

[28] J. Kofman, X. Wu, T. J. Luu, and S. Verma, "Teleoperation of a robot manipulator using a vision-based human-robot interface," *IEEE transactions on industrial electronics*, vol. 52, no. 5, pp. 1206–1219, 2005.

[29] D. Rakita, B. Mutlu, and M. Gleicher, "A motion retargeting method for effective mimicry-based teleoperation of robot arms," in *Proceedings of the 2017 ACM/IEEE International Conference on Human-Robot Interaction*, 2017, pp. 361–370.

[30] A. Ajoudani, N. Tsagarakis, and A. Bicchi, "Tele-impedance: Teleoperation with impedance regulation using a body–machine interface," *The International Journal of Robotics Research*, vol. 31, no. 13, pp. 1642–1656, 2012.

[31] K. Hashtrudi-Zaad and S. E. Salcudean, "Analysis of control architectures for teleoperation systems with impedance/admittance master and slave manipulators," *The International Journal of Robotics Research*, vol. 20, no. 6, pp. 419–445, 2001.

[32] Z. Lu, P. Huang, and Z. Liu, "High-gain nonlinear observer-based impedance control for deformable object cooperative teleoperation with nonlinear contact model," *International Journal of Robust and Nonlinear Control*, vol. 30, no. 4, pp. 1329–1350, 2020.

[33] M. Maaref, A. Rezazadeh, K. Shamaei, and M. Tavakoli, "A gaussian mixture framework for co-operative rehabilitation therapy in assistive impedance-based tasks," *IEEE journal of selected topics in signal processing*, vol. 10, no. 5, pp. 904–913, 2016.

[34] A. Haddadi and K. Hashtrudi-Zaad, "Bounded-impedance absolute stability of bilateral teleoperation control systems," *IEEE Transactions on Haptics*, vol. 3, no. 1, pp. 15–27, 2009.

[35] E. Triantafyllidis, C. Mcgrea, J. Gu, and Z. Li, "Study of multimodal interfaces and the improvements on teleoperation," *IEEE Access*, vol. 8, pp. 78 213–78 227, 2020.

[36] M. Massimino and T. Sheridan, "Variable force and visual feedback effects on teleoperator man/machine performance," in *Proceedings of the NASA Conference on Space Telerobotic*, 1989, pp. 1751–1756.

[37] M. J. Massimino and T. B. Sheridan, "Teleoperator performance with varying force and visual feedback," *Human factors*, vol. 36, no. 1, pp. 145–157, 1994.

[38] D. Senkal and H. Gurocak, "Haptic joystick with hybrid actuator using air muscles and spherical mr-brake," *Mechatronics*, vol. 21, no. 6, pp. 951–960, 2011.

[39] Y.-J. Nam and M.-K. Park, "Virtual excavator simulator featuring hils and haptic joysticks," *Journal of Mechanical Science and Technology*, vol. 29, no. 1, pp. 397–407, 2015.

[40] J. Perret and E. Vander Poorten, "Touching virtual reality: a review of haptic gloves," in *ACTUATOR 2018; 16th International Conference on New Actuators*. VDE, 2018, pp. 1–5.

[41] M. Zhu, Z. Sun, Z. Zhang, Q. Shi, T. He, H. Liu, T. Chen, and C. Lee, "Haptic-feedback smart glove as a creative human-machine interface (hmi) for virtual/augmented reality applications," *Science Advances*, vol. 6, no. 19, p. eaaz8693, 2020.

[42] J. Perret and E. Vander Poorten, "Commercial haptic gloves," in *Proceedings of the 15th Annual EuroVR Conference*. VTT Technology, 2018, pp. 39–48.

[43] T. Murakami, T. Person, C. L. Fernando, and K. Minamizawa, "Altered touch: miniature haptic display with force, thermal and tactile feedback for augmented haptics," in *ACM SIGGRAPH 2017 Posters*, 2017, pp. 1–2.

[44] J. D'Abbraccio, L. Massari, S. Prasanna, L. Baldini, F. Sorgini, G. Airò Farulla, A. Bulletti, M. Mazzoni, L. Capineri, A. Menciassi *et al.*, "Haptic glove and platform with gestural control for neuromorphic tactile sensory feedback in medical telepresence," *Sensors*, vol. 19, no. 3, p. 641, 2019.

[45] T. Bakker, J. Verlinden, D. Abbink, and R. van Deventer, "Development of a haptic device with tactile and proprioceptive feedback for spatial design tasks," in *2017 IEEE International Symposium on Mixed and Augmented Reality (ISMAR-Adjunct)*. IEEE, 2017, pp. 223–228.

[46] R. Chaudhari, C. Schuwerk, M. Danaei, and E. Steinbach, "Perceptual and bitrate-scalable coding of haptic surface texture signals," *IEEE Journal of Selected Topics in Signal Processing*, vol. 9, no. 3, pp. 462–473, 2014.

[47] C. Mizera, T. Delrieu, V. Weistroffer, C. Andriot, A. Decatoire, and J.-P. Gazeau, "Evaluation of hand-tracking systems in teleoperation and virtual dexterous manipulation," *IEEE Sensors Journal*, vol. 20, no. 3, pp. 1642–1655, 2019.

[48] G. S. Gupta, S. C. Mukhopadhyay, C. H. Messom, and S. N. Demidenko, "Master–slave control of a teleoperated anthropomorphic robotic arm with gripping force sensing," *IEEE Transactions on Instrumentation and Measurement*, vol. 55, no. 6, pp. 2136–2145, 2006.

[49] G. Zhu, X. Xiao, C. Li, J. Ma, G. Ponraj, A. Prituja, and H. Ren, "A bimanual robotic teleoperation architecture with anthropomorphic hybrid grippers for unstructured manipulation tasks," *Applied Sciences*, vol. 10, no. 6, p. 2086, 2020.

[50] M. Ye, C. Yang, V. Stankovic, L. Stankovic, and A. Kerr, "A depth camera motion analysis framework for tele-rehabilitation: Motion capture and person-centric kinematics analysis," *IEEE Journal of Selected Topics in Signal Processing*, vol. 10, no. 5, pp. 877–887, 2016.

[51] P. K. Artemiadis and K. J. Kyriakopoulos, "An emg-based robot control scheme robust to time-varying emg signal features," *IEEE Transactions on Information Technology in Biomedicine*, vol. 14, no. 3, pp. 582–588, 2010.

[52] P. Artermiadis, "Emg-based robot control interfaces: past, present and future," *Advances in Robotics & Automation*, vol. 1, no. 2, pp. 1–3, 2012.

[53] K. Gui, H. Liu, and D. Zhang, "A practical and adaptive method to achieve emg-based torque estimation for a robotic exoskeleton," *IEEE/ASME Transactions on Mechatronics*, vol. 24, no. 2, pp. 483–494, 2019.

[54] T. Teramae, T. Noda, and J. Morimoto, "Emg-based model predictive control for physical human–robot interaction: Application for assist-as-needed control," *IEEE Robotics and Automation Letters*, vol. 3, no. 1, pp. 210–217, 2017.

[55] B. Xu, W. Li, X. He, Z. Wei, D. Zhang, C. Wu, and A. Song, "Motor imagery based continuous teleoperation robot control with tactile feedback," *Electronics*, vol. 9, no. 1, p. 174, 2020.

[56] S. Zhao, Z. Li, R. Cui, Y. Kang, F. Sun, and R. Song, "Brain–machine interfacing-based teleoperation of multiple coordinated mobile robots," *IEEE Transactions on Industrial Electronics*, vol. 64, no. 6, pp. 5161–5170, 2016.

[57] S. Qiu, Z. Li, W. He, L. Zhang, C. Yang, and C.-Y. Su, "Brain–machine interface and visual compressive sensing-based teleoperation control of an exoskeleton robot," *IEEE Transactions on Fuzzy Systems*, vol. 25, no. 1, pp. 58–69, 2016.

[58] Y. Liu, W. Su, Z. Li, G. Shi, X. Chu, Y. Kang, and W. Shang, "Motor-imagery-based teleoperation of a dual-arm robot performing manipulation tasks," *IEEE Transactions on Cognitive and Developmental Systems*, vol. 11, no. 3, pp. 414–424, 2018.

[59] Y. Liu, M. Habibnezhad, and H. Jebelli, "Brain-computer interface for hands-free teleoperation of construction robots," *Automation in Construction*, vol. 123, p. 103523, 2021.

[60] B. Fang, F. Sun, H. Liu, and D. Guo, "A novel data glove using inertial and magnetic sensors for motion capture and robotic arm-hand teleoperation," *Industrial Robot: An International Journal*, 2017.

[61] Q. He, Y. Wu, Z. Feng, W. Fan, Z. Lin, C. Sun, Z. Zhou, K. Meng, W. Wu, and J. Yang, "An all-textile triboelectric sensor for wearable teleoperated human–machine interaction," *Journal of Materials Chemistry A*, vol. 7, no. 47, pp. 26 804–26 811, 2019.

[62] G. Cheung, D. Florencio, P. Le Callet, C.-W. Lin, and E. Magli, "Introduction to the issue on interactive media processing for immersive communication," *IEEE Journal of Selected Topics in Signal Processing*, vol. 9, no. 3, pp. 381–383, 2015.

[63] C. P. Vo, X. D. To, and K. K. Ahn, "A novel force sensorless reflecting control for bilateral haptic teleoperation system," *IEEE Access*, vol. 8, pp. 96 515–96 527, 2020.

[64] W. Qi, X. Liu, L. Zhang, L. Wu, W. Zang, and H. Su, "Adaptive sensor fusion labeling framework for hand pose recognition in robot teleoperation," *Assembly Automation*, 2021.

[65] A. Dong, Z. Du, and Z. Yan, "A sensorless interaction forces estimator for bilateral teleoperation system based on online sparse gaussian process regression," *Mechanism and Machine Theory*, vol. 143, p. 103620, 2020.

[66] R. Uddin and J. Ryu, "Predictive control approaches for bilateral teleoperation," *Annual Reviews in Control*, vol. 42, pp. 82–99, 2016.

[67] S. Munir and W. J. Book, "Internet based teleoperation using wave variables with prediction," in *2001 IEEE/ASME International Conference on Advanced Intelligent Mechatronics. Proceedings (Cat. No. 01TH8556)*, vol. 1. IEEE, 2001, pp. 43–50.

[68] K. Hauser, "Recognition, prediction, and planning for assisted teleoperation of freeform tasks," *Autonomous Robots*, vol. 35, no. 4, pp. 241–254, 2013.

[69] B. Xi, S. Wang, X. Ye, Y. Cai, T. Lu, and R. Wang, "A robotic shared control teleoperation method based on learning from demonstrations," *International Journal of Advanced Robotic Systems*, vol. 16, no. 4, p. 1729881419857428, 2019.

[70] C. Smith and P. Jensfelt, "A predictor for operator input for time-delayed teleoperation," *Mechatronics*, vol. 20, no. 7, pp. 778–786, 2010.

[71] K. Hosseini-Suny, H. Momeni, and F. Janabi-Sharifi, "Model reference adaptive control design for a teleoperation system with output prediction," *Journal of Intelligent & Robotic Systems*, vol. 59, no. 3, pp. 319–339, 2010.

[72] M. Nikpour, B. Yazdankhoo, B. Beigzadeh, and A. Meghdari, "Adaptive online prediction of operator position in teleoperation with unknown time-varying delay: simulation and experiments," *Neural Computing and Applications*, pp. 1–18, 2020.

[73] J.-Q. Huang and F. L. Lewis, "Neural-network predictive control for nonlinear dynamic systems with time-delay," *IEEE Transactions on Neural Networks*, vol. 14, no. 2, pp. 377–389, 2003.

[74] H. Wang, P. X. Liu, and S. Liu, "Adaptive neural synchronization control for bilateral teleoperation systems with time delay and backlash-like hysteresis," *IEEE transactions on cybernetics*, vol. 47, no. 10, pp. 3018–3026, 2017.

[75] M. Ewerthon, G. Maeda, D. Koert, Z. Kolev, M. Takahashi, and J. Peters, "Reinforcement learning of trajectory distributions: Applications in assisted teleoperation and motion planning," in *2019 IEEE/RSJ International Conference on Intelligent Robots and Systems (IROS)*. IEEE, 2019, pp. 4294–4300.

[76] K. Kamali, I. A. Bonev, and C. Desrosiers, "Real-time motion planning for robotic teleoperation using dynamic-goal deep reinforcement learning," in *2020 17th Conference on Computer and Robot Vision (CRV)*. IEEE, 2020, pp. 182–189.

[77] A. Agrawal, "Automating endoscopic camera motion for teleoperated minimally invasive surgery using inverse reinforcement learning," Ph.D. dissertation, Master's thesis, Worcester Polytechnic Institute, 2018.

[78] D. R. Scobee, V. R. Royo, C. J. Tomlin, and S. S. Sastry, "Haptic assistance via inverse reinforcement learning," in *2018 IEEE International Conference on Systems, Man, and Cybernetics (SMC)*. IEEE, 2018, pp. 1510–1517.

[79] T. Zhang, Z. McCarthy, O. Jow, D. Lee, X. Chen, K. Goldberg, and P. Abbeel, "Deep imitation learning for complex manipulation tasks from virtual reality teleoperation," in *2018 IEEE International Conference on Robotics and Automation (ICRA)*. IEEE, 2018, pp. 5628–5635.

[80] D. J. Brown and M. J. Proulx, "Audio–vision substitution for blind individuals: Addressing human information processing capacity limitations," *IEEE Journal of Selected Topics in Signal Processing*, vol. 10, no. 5, pp. 924–931, 2016.

[81] O. Dena, T. Faghani, and A. H. Aghvami, "Gbdt-based modules for force prediction in a model-mediated teleoperation system," in *2020 27th International Conference on Telecommunications (ICT)*. IEEE, 2020, pp. 1–6.

[82] A. Haddadi and K. Hashturdi-Zaad, "Robust stability of teleoperation systems with time delay: A new approach," *IEEE transactions on haptics*, vol. 6, no. 2, pp. 229–241, 2012.

[83] A. Handa, K. Van Wyk, W. Yang, J. Liang, Y.-W. Chao, Q. Wan, S. Birchfield, N. Ratliff, and D. Fox, "Dexpilot: Vision-based teleoperation of dexterous robotic hand-arm system," in *2020 IEEE International Conference on Robotics and Automation (ICRA)*. IEEE, 2020, pp. 9164–9170.

[84] O. M. Andrychowicz, B. Baker, M. Chociej, R. Jozefowicz, B. McGrew, J. Pachocki, A. Petron, M. Plappert, G. Powell, A. Ray *et al.*, "Learning dexterous in-hand manipulation," *The International Journal of Robotics Research*, vol. 39, no. 1, pp. 3–20, 2020.

[85] S. Cruciani, B. Sundaralingam, K. Hang, V. Kumar, T. Hermans, and D. Kragic, "Benchmarking in-hand manipulation," *IEEE Robotics and Automation Letters*, vol. 5, no. 2, pp. 588–595, 2020.

[86] M. Li, H. Yin, K. Tahara, and A. Billard, "Learning object-level impedance control for robust grasping and dexterous manipulation," in *2014 IEEE International Conference on Robotics and Automation (ICRA)*. IEEE, 2014, pp. 6784–6791.

[87] X. Gu, Y. Zhang, W. Sun, Y. Bian, D. Zhou, and P. O. Kristensson, "Dexmo: An inexpensive and lightweight mechanical exoskeleton for motion capture and force feedback in vr," in *Proceedings of the 2016 CHI Conference on Human Factors in Computing Systems*, 2016, pp. 1991–1995.

[88] S. V. Shah, S. K. Saha, and J. K. Dutt, "Dynamics of tree-type robotic systems," in *Dynamics of Tree-Type Robotic Systems*. Springer, 2013, pp. 73–88.

[89] V. R. Kumar and K. J. Waldron, "Force distribution in closed kinematic chains," *IEEE Journal on Robotics and Automation*, vol. 4, no. 6, pp. 657–664, 1988.

[90] J. K. Davidson, K. H. Hunt, and G. R. Pennock, "Robots and screw theory: applications of kinematics and statics to robotics," *J. Mech. Des.*, vol. 126, no. 4, pp. 763–764, 2004.

[91] Y. Zhang, F. Gao, and W. A. Gruver, "Determination of contact forces in grasping," in *Proceedings of IEEE/RSJ International Conference on Intelligent Robots and Systems. IROS'96*, vol. 3. IEEE, 1996, pp. 1038–1044.

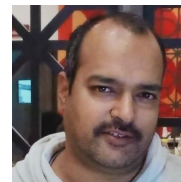
[92] R. Kumar and S. Mukherjee, "Enhanced dynamic capability of cable-driven parallel manipulators by reconfiguration," *Robotica*, pp. 1–19, 2021.

[93] J. C. A. Barata and M. S. Hussein, "The moore–penrose pseudoinverse: A tutorial review of the theory," *Brazilian Journal of Physics*, vol. 42, no. 1-2, pp. 146–165, 2012.

- [94] B. Siciliano and O. Khatib, *Springer handbook of robotics*. Springer, 2016.
- [95] J. Mäkinen, "Rotation manifold $so(3)$ and its tangential vectors," *Computational Mechanics*, vol. 42, no. 6, pp. 907–919, 2008.
- [96] J.-L. Blanco, "A tutorial on $se(3)$ transformation parameterizations and on-manifold optimization," *University of Malaga, Tech. Rep.*, vol. 3, p. 6, 2010.
- [97] M. Zefran, V. Kumar, and C. B. Croke, "On the generation of smooth three-dimensional rigid body motions," *IEEE Transactions on Robotics and Automation*, vol. 14, no. 4, pp. 576–589, 1998.
- [98] M. F. Sani and G. Karimian, "Automatic navigation and landing of an indoor ar. drone quadrotor using aruco marker and inertial sensors," in *2017 international conference on computer and drone applications (ICoDa)*. IEEE, 2017, pp. 102–107.
- [99] L. Ruiz, F. Gama, and A. Ribeiro, "Gated graph recurrent neural networks," *IEEE Transactions on Signal Processing*, vol. 68, pp. 6303–6318, 2020.
- [100] Y. She, Y. He, and D. Wu, "Learning topology and dynamics of large recurrent neural networks," *IEEE Transactions on Signal Processing*, vol. 62, no. 22, pp. 5881–5891, 2014.
- [101] Y. Xia, "A compact cooperative recurrent neural network for computing general constrained l_1 norm estimators," *IEEE transactions on signal processing*, vol. 57, no. 9, pp. 3693–3697, 2009.
- [102] L. Zhang, G. Wang, and G. B. Giannakis, "Real-time power system state estimation and forecasting via deep unrolled neural networks," *IEEE Transactions on Signal Processing*, vol. 67, no. 15, pp. 4069–4077, 2019.
- [103] N. Farsad and A. Goldsmith, "Neural network detection of data sequences in communication systems," *IEEE Transactions on Signal Processing*, vol. 66, no. 21, pp. 5663–5678, 2018.
- [104] I. Goodfellow, Y. Bengio, A. Courville, and Y. Bengio, *Deep learning*. MIT press Cambridge, 2016, vol. 1, no. 2.
- [105] N. M. Vural, S. Ergut, and S. S. Kozat, "An efficient and effective second-order training algorithm for lstm-based adaptive learning," *IEEE Transactions on Signal Processing*, pp. 1–1, 2021.
- [106] H. Abdi and L. J. Williams, "Principal component analysis," *Wiley interdisciplinary reviews: computational statistics*, vol. 2, no. 4, pp. 433–459, 2010.



Brejesh Lall received the B.E. and M.E. degrees in electronics and communications engineering from Delhi College of Engineering, Delhi University, in 1991 and 1992, respectively, and the Ph.D. degree in the area of multi-rate signal processing from the Indian Institute of Technology, Delhi, in 1999. His research interests are in signal and image analysis, computer vision, multimedia systems, multi-scale modelling of stochastic processing wide-sense, cyclostationary process representation physical layer in wireless communication. He has over 50 papers in international journals and refereed conferences. From September 1997 to June 2005, he worked at Hughes Software Systems, in the digital signal processing group. Since July 2005, he has been with the faculty of the Department of Electrical Engineering, Indian Institute of Technology, Delhi, where he is currently a Professor.



Arzad A. Kherani Dr. Arzad Alam Kherani is currently Associate Professor (Department of Electrical Engineering and Computer Science) at IIT, Bhilai. He has worked on broad areas of Computer networks, Queueing systems, Wireless communications. He has also worked for industry for a decade and gained experience with product conceptualization, product design and development, industrial R&D and standardization. He did Master's in 1999 and PhD in 2003 from IISc Bangalore.



Rajesh Kumar is a PhD from Indian Institute of Technology Delhi. His research focuses on Robot Kinematics, Control and AI based methods in order to improve robot autonomy. He is a B.Tech in Mechanical Engineering from Indian Institute of Technology Delhi, India.



Pimmy Gandotra received the B.E. degree in Electronics and Communication Engineering from Jammu University, Jammu and Kashmir, India, in 2013 and the M.Tech degree in Electronics and Communication Engineering from Shri Mata Vaishno Devi University in 2016. She pursued her Ph. D degree in Electronics and Communication Engineering at Shri Mata Vaishno Devi University, Katra, Jammu and Kashmir, India. Her research interest includes the emerging technologies of 5G wireless communication network. Currently she is pursuing her post-doctoral research at Indian Institute of Technology as a Principal Project Scientist. She has received teaching assistantship from MHRD from 2014-2016. She is a student member of Institute of Electrical and Electronics Engineers (IEEE).



Sudipto Mukherjee is a Professor in Department of Mechanical Engineering, Indian Institute of Technology Delhi, India. He holds a PhD and a M.Tech degree from Ohio University, USA and a B.Tech degree from Indian Institute of Technology Kanpur, India.